



TITLE:

Systematic Control of Structural Changes in GeO₂ Glass Induced by Femtosecond Laser Direct Writing

AUTHOR(S):

Asai, Taiga; Shimotsuma, Yasuhiko; Kurita, Torataro; Murata, Atsushi; Kubota, Sho; Sakakura, Masaaki; Miura, Kiyotaka; Brisset, Francois; Poumellec, Bertrand; Lancry, Matthieu

CITATION:

Asai, Taiga ...[et al]. Systematic Control of Structural Changes in GeO₂ Glass Induced by Femtosecond Laser Direct Writing. *Journal of the American Ceramic Society* 2015, 98(5): 1471-1477

ISSUE DATE:

2015-01-31

URL:

<http://hdl.handle.net/2433/198787>

RIGHT:

This is the peer reviewed version of the following article: Asai, T., Shimotsuma, Y., Kurita, T., Murata, A., Kubota, S., Sakakura, M., Miura, K., Brisset, F., Poumellec, B., Lancry, M. (2015), Systematic Control of Structural Changes in GeO₂ Glass Induced by Femtosecond Laser Direct Writing. *Journal of the American Ceramic Society*, 98: 1471–1477, which has been published in final form at <http://dx.doi.org/10.1111/jace.13482>. This article may be used for non-commercial purposes in accordance with Wiley Terms and Conditions for Self-Archiving.; 許諾条件により本文ファイルは2016-01-31に公開.; This is not the published version. Please cite only the published version.; この論文は出版社版ではありません。引用の際には出版社版をご確認ください。

Systematic control of structural changes in GeO₂ glass induced by femtosecond-laser direct writing

Taiga Asai¹, Yasuhiko Shimotsuma^{1*}, Torataro Kurita¹, Atsushi Murata¹, Sho Kubota¹, Masaaki Sakakura¹, Kiyotaka Miura¹, Francois Brisset², Bertrand Pommellec² and Matthieu Lancry²

¹ Department of Material Chemistry, Kyoto University, Kyoto, 615-8510 Japan

² ICMMO, UMR CNRS-PSUD 8182, Université Paris Sud, Bâtiment 410, 91405 Orsay, France

Abstract

We report the structural changes inside germania glass induced by femtosecond laser pulses. Inspection by polarization microscopy and secondary electron microscopy indicate that the periodic nanostructures consist of oxygen defects such as ODCs (oxygen deficient centers) and NBOHCs (non-bridging oxygen hole centers) for laser pulse energy less than 0.2 μJ . However, the glass network was dissociated and O₂ molecules were generated for laser pulse energy greater than 0.4 μJ . Two different structural-changes, form-birefringence and dissociation, were induced in GeO₂ glass, depending on the laser pulse energy. The form-birefringence exhibited by the nanogratings in GeO₂ glass is larger than that in SiO₂ glass for pulse energy less than 0.2 μJ , since the density of nanovoids enclosed by ODCs in GeO₂ glass is higher than that in SiO₂ glass. Arrhenius plots of the phase retardation caused by the nanogratings in GeO₂ and SiO₂ indicate that the oxygen defects are relaxed at a temperature 100 °C above the glass transition temperature.

* Corresponding author's e-mail address: yshimo@func.mc.kyoto-u.ac.jp

Introduction

Three dimensional Material processing at the micro- and nano-scales including ink jet, electron beam, focused ion beam and laser beam has attracted considerable interests due to a wide range of applications ranging from optical integrated circuits and microfluidics to MEMS devices.^{1,2} Furthermore, structural modification in transparent materials such as glass by direct writing with femtosecond laser pulses has a key advantage, compared to longer-pulsed lasers.³ In the last decade or so, myriad of glass interactions with femtosecond laser pulses, including surface ripples,⁴ refractive index changes,⁵ 3D self-organized sub-wavelength structures,⁶ glass decomposition,⁷ elemental distribution,⁸ nanoparticle precipitations,⁹ and non-reciprocal photosensitivity^{10,11} are demonstrated. Especially, silica and germania are two of the most commonly studied oxide glasses,¹² due to their advantageous optical properties and the simple structure composed of tetrahedral (SiO_4 or GeO_4) framework.¹³ Recently Bressel et al. reported interesting phenomena of structural changes inside GeO_2 glass induced by tightly focused femtosecond laser beam via high NA objective.¹⁴⁻¹⁶ We have also observed element distribution in silicate glasses including network modifiers under high-repetition-rate femtosecond laser irradiation.¹⁷ These results indicate that the main driving force is the sharp temperature gradient, which is originated from the thermal accumulation around the focus.¹⁸ More intriguing phenomenon in the case of SiO_2 glass is self-assembly of periodic nanostructures in the direction perpendicular to the light polarization.⁶ Such periodic nanostructures are ruled in the direction parallel to the polarization of the writing laser and consist of thin regions with a low refractive index characterized by a strong oxygen deficiency,⁶ surrounded by larger regions with a positive index change.¹⁹ As a result, self-assembled form birefringence can be observed after femtosecond laser irradiation.²⁰ As opposed

to ripple structure on the surface of the various materials (metal, semiconductor, dielectrics),²¹⁻²⁴ nanogratings inside of the material were found only for handful materials.^{25,26} Furthermore, the formation mechanism of nanogratings is still a mystery.^{6,7,27} More recently, we have first observed the formation of the polarization-dependent nanograting structures indicating form-birefringence inside GeO₂ glass.²⁸ Subsequently, Zhang et al. have also confirmed that birefringence derived from the self-organized nanogratings in GeO₂ glass can be controlled by adjusting laser pulse energy.²⁹ Here, by using GeO₂ glass, we report that systematic control of structural changes, ranging from the formation of nanogratings to the destruction of Ge-O bonds in glass matrix, according to increase in laser pulse energy.

Experimental Procedure

The GeO₂ glass sample was prepared from GeO₂ powder (Aldrich; 99.999 %) by melting at 1600 °C in a platinum crucible for 3 h. And then the melt in the crucible was cooled down to room temperature in air. The formed glass was then annealed at 500 °C for 6 h to relieve the residual stress. Transparent and bubble free glass was obtained, and polished for further experiments. Between the experiments, GeO₂ glass samples were stored in a desiccator because of the hygroscopic properties of this glass.

In the experiments, a mode-locked, regeneratively amplified Ti:Al₂O₃ laser system (Coherent; RegA 9000), operating at 800 nm with 50 fs pulse duration and 250 kHz repetition rate was used. The laser beam was focused via a microscope objective (Nikon; LU Plan Fluor, 50× 0.80 N.A.) at a depth of about 100 μm below the GeO₂ glass sample surface. The pulse energy was controlled by a variable neutral density filter (0.08 ~ 2.4 μJ). The linear polarization orientation of laser beam

was rotated by a half-wave plate. The typical irradiation time was 1 s (250000 pulses). After laser irradiation, the modified region was inspected by an optical microscope, a polarization microscope (CRi; LC-Polscope), and a confocal Raman spectrometer excited by DPSS laser with a wavelength of 532 nm (Tokyo Instrument; NanoFinder 30). After etching the sample surface to the depth of the beam waist location by using a focused ion beam (FIB, JEOL; JIB-4600F), the surface was analyzed by a scanning electron microscope (SEM). In addition, to elucidate the structural relaxation of the modified region in glass, the sample after the laser irradiation was successively annealed at various temperatures for 1 h. To probe the matter within the nanoplanes, we decided to cleave the samples along the nanostructure plans. We then analyzed the laser tracks exposed within these cleaves using a Field-Emission Gun Scanning Electron Microscope (FEG-SEM ZEISS SUPRA 55 VP). Some of these FEG-SEM allows the examination of native uncoated insulating or dielectric specimens using low accelerating voltage (typically in the range of 1 kV) and very low current (a few pA) because they can keep an image resolution sufficiently high even under these extreme conditions. Thus the original characteristics of the samples may be preserved for further testing or manipulation since no conductive coating is required.

Results and Discussion

Fig. 1 shows the optical microscope images from top and side view of the modified region inside GeO_2 glass after the femtosecond laser irradiation with various pulse energies. For pulse energy less than 0.2 μJ , the modified structures were similar to the structural change inside fused silica produced by the femtosecond laser irradiation. Such teardrop-shaped structure extending along the optical axis was mainly derived from the spherical aberration due to the refractive index mismatch

between the air and the glass. The relationship between the focal displacement Δ (the largest distance between the focal spots by the paraxial rays and the off-axis rays) and the focusing depth f_d is described by the following equation:³⁰

$$\Delta = \frac{f_d}{n} \left(\sqrt{\frac{n^2 - \text{NA}^2}{1 - \text{NA}^2}} - n \right) \quad (1)$$

where NA is the numerical aperture of the objective, n is the refractive index of the sample. Compared with the induced structure inside SiO_2 glass at the same pulse energy, the modified structure inside GeO_2 glass was longer owing to the higher refractive index of GeO_2 .³¹ For pulse energy greater than 0.4 μJ , which is much higher than the self-focusing threshold, the modified regions consisted of the teardrop-shaped inner region and the surrounding outer elliptical region. The inner regions were composed of color centers and bubbles from the breakdown of glass structure, indicating that such structural changes are produced by the extremely high temperature and pressure derived from the laser pulses.³² In the outer region, the much larger structural modification of GeO_2 glass melting compared to the focal volume was likely formed by the thermal accumulation via the conduction of the heat transferred from the laser-excited electrons to the lattice. Although such melting region is no apparent in SiO_2 glass for similar repetition rate, this phenomenon was remarkable when femtosecond laser pulses with high pulse repetition rate were focused inside multi-component silicate glass.³³

To reveal the structural changes inside glass, Raman spectra of the modified region after the laser irradiation were measured as shown in Fig. 2. To emphasize the difference between Raman spectra depending on the various laser energy, the vertical axis was plotted with logarithmic scale. Typical

main peak at 420 cm^{-1} is assigned to the symmetric stretching vibration of Ge-O-Ge in predominantly six-membered rings. The weak peak at the low-wavenumber side of the main peak ($\sim 345\text{ cm}^{-1}$) presents the motion of Ge with little O motion. The broad shoulder at 520 cm^{-1} (D2 band) is attributed to the breathing of 3-membered rings of $(\text{GeO})_3$. Other features of the Raman spectrum of GeO_2 glass show two peaks at 860 and 970 cm^{-1} , which are attributed to the TO and LO asymmetric stretching modes of bridging oxygens, respectively.¹² Furthermore, the “high-wavenumber” peak at 1555 cm^{-1} , which is attributed to a molecular O_2 ,¹⁶ was observed after the irradiation of femtosecond laser with higher pulse energy than $0.2\text{ }\mu\text{J}$ as observed for SiO_2 .⁷ This implies that O_2 molecules were locally generated inside GeO_2 glass by the femtosecond laser irradiation, which is good agreement with previous work reported in Ref. 16. In order to clarify the “degree” of the structural change depending on the laser pulse energy, the Raman peak ratios with respect to the initial intensities at 420 , 520 , and 1555 cm^{-1} were plotted as a function of the pulse energy (Fig. 2 inset). When the pulse energy is lower than $0.4\text{ }\mu\text{J}$, the ratio at 520 cm^{-1} was slightly increased with increase in the laser pulse energy, and then this ratio was decreased. It should be noted that D2 peak intensity is sensitive to the main peak intensity. In contrast the ratio at 1555 cm^{-1} was increased proportionally and saturated at the pulse energy larger than $1.6\text{ }\mu\text{J}$. The decrease of the ratio at 420 cm^{-1} indicates the disruption of symmetry around the Ge-O-Ge.²⁹

The spatial distribution of the structural change was also revealed by the confocal Raman spectral mapping.²⁸ In the case of low pulse energy of $0.08\text{ }\mu\text{J}$, a slight decrease of peak intensity at 420 cm^{-1} was observed at the focus position. Meanwhile, the peak intensities at 520 and 1555 cm^{-1} were slightly increased. On the other hand, in the case of high laser pulse energy of $2.4\text{ }\mu\text{J}$, the Raman intensities at 420 and 520 cm^{-1} in the central part of focus were decreased. The decrease of

these two peaks was distributed along the laser propagation direction. Furthermore, the intensity at 1555 cm^{-1} was increased at the focus, implying that the molecular O_2 was generated. It should be noted that D2 peak intensity around the outer boundary was increased. Such structural densification around the photoexcited region, in which viscoelastic strain was induced, is caused by the compression based on the glass thermal expansion.^{17,33}

The photoinduced birefringence around the photoexcited region by the femtosecond laser with various pulse energy was observed with a polarization microscope.²⁸ As it is the case with SiO_2 glass, the polarization-dependent form birefringence was observed in the center part of focus for pulse energies lower than $0.4\text{ }\mu\text{J}$. The slow axis orientation is aligned perpendicularly to the laser polarization direction, implying that the nanogratings could be also created inside glass in this pulse energy range. While, for pulse energy greater than $0.8\text{ }\mu\text{J}$, the smaller phase retardation corresponding to the lower brightness around the focus regions was observed. Furthermore, the slow axis in the outer regions of viscoelastic strain were radially-oriented, indicating that the heat-modified region has been compressed due to the thermal expansion during the laser irradiation.³⁴ Tensile stress was thus generated in the surroundings of the modified regions, which resulted in the concentrically oriented slow axis.

We have also measured the variation of the birefringence retardation induced by the femtosecond laser pulses with various pulse repetition rate (R_{pulse}) and pulse duration (τ_{pulse}) (Fig. 3). In these experiments, we used a mode-locked, regeneratively amplified Yb:KGW laser system (Light Conversion; Pharos), operating at 1030 nm . For $R_{\text{pulse}} < 200\text{ kHz}$, the phase retardation increased

with increasing R_{pulse} , and became asymptotically constant for $R_{\text{pulse}} \geq 200$ kHz. This could be explained by the occurrence of a thermal accumulation effect within the focal volume when the R_{pulse} is greater than ~ 200 kHz.³⁵ This indicates that the pulse energy range to produce self-assembled nanogratings narrows when the R_{pulse} increases. Although slight increase of phase retardation at about 1 ps was observed, the retardation decreased with increasing τ_{pulse} within our study range. This is explained by the previous opinion that for the 4 ps pulses with 20 times lower peak intensity than the intensity of the 200 fs pulses, the process of glass modification leading to the formation of nanogratings is more susceptible to the presence of defects such as the non-bridging oxygen hole center (NBOHC).³⁶ For SiO₂ glass in $\tau_{\text{pulse}} < 200$ fs, although the periodicity of nanograting was independent of τ_{pulse} ,³⁷ in contrast, Stoian et al. have effectively shown that the nanogratings periodicity decreases up to τ_{pulse} of 700fs, based on the blue light diffraction efficiency.³⁸

To confirm absolute proof of the nanogratings formation inside GeO₂ glass, SEM observations of the modified regions were performed after dry etching by FIB, because GeO₂ glass has a solubility in water of ~ 4.5 g/L. Secondary electron images (SEIs) and backscattering electron images (BEIs) of the same surface were compared (Fig. 4). It is well known that the SEIs reveal mainly the surface morphology of a sample, while the BEIs are more sensitive to the atomic weight of the elements or the density of material constituting the observation surface. The SEIs of the etched GeO₂ glass sample indicate that the morphology of an irradiated sample in the examined cross section almost does not change. On the other hand, the BEIs (Fig. 4 (b), (d)) reveal a reasonably good periodic structure of stripe-like dark regions with low density of material and of 50 nm width which are aligned perpendicular to the writing laser polarization direction. Horizontal striation, slightly

visible in the SEIs (Fig. 4 (a), (c)), could be explained by unusual self-organization of nanovoids⁷ or a weak surface relief created in the etching process. Such nanoporous structures characterized by glass decomposition³⁹ with oxygen release into nanopores have been confirmed recently using small angle X-ray scattering⁴⁰ and TEM.⁴¹

To confirm the detailed of nanograting structure, we have also observed the sample surface cleaved along the nanostructure planes using a Field-Emission Gun Scanning Electron Microscope (FEG-SEM ZEISS SUPRA 55 VP).³⁹ Such observations by using a low accelerating voltage and very low current reveal the original characteristics of the sample surface without a conductive coating. Fig. 5 shows SEIs on the cleaved surface of the laser traces written by the femtosecond laser pulses with different pulse energy for each writing laser polarization. In the case of low pulse energy of 0.2 μJ (Fig. 5 (a), (b)), the SEIs apparently show the nanograting structures corresponding to areas of density contrast (Fig. 4 (b), (d)) leading to the refractive index modulation. When the laser polarization is along the writing direction, nanopores with the diameter of ~ 10 nm were observed within the nanoplanes (Fig. 5 (c), (d)). Evidently, these nanogratings consisting of mesoporous nanoplanes were self-aligned perpendicular to the laser polarization. As a result, such nanogratings are at the origin of the strong refractive index contrast leading to the optical anisotropy. On the other hand, in the case of high pulse energy of 2.4 μJ , hollow structure with multiple large voids with the size of several micrometers were formed (Fig. 5 (f), (h)). Considering that the molecular O_2 was generated (Fig. 2), these voids can be produced as a result of decomposition of GeO_2 to $\text{GeO}_{(2-x)} + x/2 \cdot \text{O}_2$ in the same manner as SiO_2 glass.⁶ To reveal the difference in the nanograting structures for GeO_2 and SiO_2 , the cleaved sample surface of the modified regions in GeO_2 and

SiO₂ were observed (Fig. 6). Superficially regarded, the average size of nanopores in GeO₂ glass (< 10nm) was slightly smaller than that in SiO₂ glass (10 ~ 30nm),⁷ though their packing density seems to be higher. It's well known that the strength of form birefringence depends on the nanogratings periodicity, layers thickness and the refractive indices of these two layers. The birefringence of nanogratings for ordinary (n_o) and extraordinary (n_e) wave is:⁴²

$$\Delta n = n_e - n_o = \sqrt{fn_1^2 + (1-f)n_2^2} - \frac{n_1 n_2}{\sqrt{fn_2^2 + (1-f)n_1^2}} \quad (2)$$

where f is the filling factor, n_1 and n_2 are the unknown refractive indices for the platelets constituting the nanograting. As shown in Fig. 7, these periodic structures are ruled in the direction parallel to the polarization of the writing laser and consist of thin regions of index of refraction n_1 , characterized by a strong oxygen deficiency,⁶ surrounded by larger regions of index n_2 . In addition, based on the Maxwell-Garnett theory, the effective refractive index (n_1) of the mesoporous panoplanes with the thickness of 50nm for GeO₂ glass is:⁴³

$$n_1^2 = n_{defect}^2 \left\{ 1 - \frac{3\phi(n_{defect}^2 - n_{pore}^2)}{2n_{defect}^2 + n_{pore}^2 + \phi(n_{defect}^2 - n_{pore}^2)} \right\} \quad (3)$$

where ϕ is the porosity, n_{pore} (= 1) and n_{defect} are the local refractive indices for the nanopores and for the surrounding oxygen defect regions, respectively.

After measuring the thickness of L of nanograting structures in the direction of the propagation of light by using crossed-Nicols, we have also evaluated the birefringence from the phase retardation which is measured by polarization microscope (Fig. 8). Although the phase retardation for both GeO₂ and SiO₂ increases with increasing the pulse energy, this value for GeO₂ started to decrease at 0.4 μ J, owing to the glass decomposition. In the case of SiO₂, this peak was at about 1 μ J. It

should be noted that the birefringence for GeO₂ monotonically decreased with increasing in the pulse energy, in contrast to the change in the case of SiO₂. It is possible to induce a higher birefringence for GeO₂ at lower pulse energy, compared to SiO₂. Indeed, the birefringence for SiO₂ and GeO₂ at the laser pulse energy of 0.12 μJ were 0.003 and 0.005, respectively. Assuming the reasonable numbers of n_{defect} and ϕ , based on the very slight refractive index change due to the oxygen deficiencies,⁴⁴ we found that our experimental results are in good agreement with previous studies.¹⁹ The parameters for calculation and the obtained results were listed in Table 1.

In order to speculate the thermal stabilities of the photoinduced structures inside GeO₂ glass from the birefringence changes according to the annealing temperature, an isochronal annealing experiment was performed (Fig. 9). The birefringent regions were still clearly visible under a polarization microscope even after annealing at 873 K (Fig. 9(a)). On the contrary, in the case of high pulse energy of 2.4 μJ, the internal stress distribution around the modified regions disappeared after an annealing at 823 K within 1 hour (Fig. 9(b)). These results indicate that the birefringent structures constituted by oxygen deficiencies⁶ and nanopores are relaxed completely by the annealing at the temperature, which is about 100 K higher than glass transition point ($T_g \sim 823$ K). In contrast, in the case of high pulse energy, the center region still remained a hollow structure after annealing at 823 K. To compare the thermal stabilities of nanogratings between GeO₂ and SiO₂, the amount of the induced phase retardation were plotted against inverse temperature based on Arrhenius equation:

$$\frac{R_0 - R}{R_0} = A \exp\left(-\frac{E_a}{\kappa_B T}\right) \quad (4)$$

where R_0 and R is the initial phase retardation of the birefringent structure and the phase retardation after successive annealing at various temperature, respectively. E_a is the activation energy for birefringence relaxation, A is the frequency factor, T is the absolute temperature, and κ_B is the Boltzmann constant. In good agreement with the previously reported results^{45,46} the best linear fit was obtained with activation energy of 0.2 eV or 1.9 eV for GeO_2 or SiO_2 , respectively. These results imply that the birefringence relaxation is originated from the oxygen vacancy annihilation.

Conclusions

We have confirmed the formation of the nanograting structures inside GeO_2 glass for pulse energy less than 0.2 μJ . Similarly to SiO_2 glass, nanograting structures consisting of mesoporous nanoplanes with the thickness of 50 nm, were self-organized in the direction perpendicular to the laser polarization. Such nanogratings is completely erased by the annealing at the temperature which is about 100 K higher than glass transition temperature. For pulse energy greater than 0.4 μJ , the destruction of Ge-O bonds in glass matrix occurred and then O_2 molecules were generated inside focal volume. We anticipate that such embedded nanograting structures and dissociated microstructure in GeO_2 glass could be applied to optical storage, waveguide, and other micro-devices.

Acknowledgements

This work was financially supported by JSPS KAKENHI Grant Number 26630129. We would like to thank Prof. Kazuyuki Hirao from Kyoto University, Prof. Peter G. Kazansky from University of Southampton and Prof. Jianrong Qiu from South China University of Technology for their kind

suggestions and discussions. This work has been performed in the frame of FLAG (Femtosecond Laser Application in Glasses) consortium project with the support of the Agence Nationale pour la Recherche (ANR-09-BLAN-0172-01) and FP7-PEOPLE-IRSES e-FLAG 247635.

References

1. S. Kawata, H. –B. Sun, T. Tanaka, and K. Takada, “Finer features for functional microdevices,” *Nature* **412** [6848] 697-698 (2001).
2. M. Farsari and B. N. Chichkov, “Materials processing: Two-photon fabrication,” *Nat. Photon.* **3** [8] 450-452 (2009).
3. B. C. Stuart, M. D. Feit, A. M. Rubenchik, B. W. Shore, and M. D. Perry, “Laser-induced damage in dielectrics with nanosecond to subpicosecond pulses” *Phys. Rev. Lett.* **74** [12] 2248-2251 (1995).
4. J. Bonse, J. Krüger, S. Höhm, and A. Rosenfeld, “Femtosecond laser-induced periodic surface structures,” *J. Laser Appl.* **24** [4] 042006 7pp. (2012).
5. K. M. Davis, K. Miura, N. Sugimoto, and K. Hirao, “Writing waveguides in glass with a femtosecond laser,” *Opt. Lett.* **21** [21] 1729-1731 (1996).
6. Y. Shimotsuma, P. Kazansky, J. Qiu, and K. Hirao, “Self-organized nanogratings in glass irradiated by ultrashort light pulses,” *Phys. Rev. Lett.* **91** [24] 247405 4pp. (2003).
7. M. Lancry, B. Pommellec, J. Canning, K. Cook, J. -C. Poulin, and F. Brisset, “Ultrafast nanoporous silica formation driven by femtosecond laser irradiation,” *Laser Photon. Rev.* **7** [6] 953-962 (2013).
8. M. Sakakura, T. Kurita, M. Shimizu, K. Yoshimura, Y. Shimotsuma, N. Fukuda, K. Hirao, and

- K. Miura, "Shape control of elemental distributions inside a glass by simultaneous femtosecond laser irradiation at multiple spots," *Opt. Lett.* **38** [23] 4939-4942 (2013).
9. J. Qiu, X. Jiang, C. Zhu, M. Shirai, J. Si, N. Jiang, and K. Hirao, "Manipulation of gold nanoparticles inside transparent materials," *Angew. Chem., Int. Ed.* **43** [17] 2230-2234 (2004).
 10. P. G. Kazansky, W. Yang, E. Bricchi, J. Bovatsek, A. Arai, Y. Shimotsuma, K. Miura, and K. Hirao, " "Quill" writing with ultrashort light pulses in transparent materials," *Appl. Phys. Lett.* **90** [15] 151120 3pp. (2007).
 11. B. Poumellec, M. Lancry, J. -C. Poulin, and S. Ani-Joseph, "Non reciprocal writing and chirality in femtosecond laser irradiated silica," *Opt. Express* **16** [22] 18354-18361 (2008).
 12. G. S. Henderson, D. R. Neuville, B. Cochain, and L. Cormier, "The structure of $\text{GeO}_2\text{-SiO}_2$ glasses and melts: A Raman spectroscopy study," *J. Non-Cryst. Solids* **355** [8] 468-474 (2009).
 13. W. H. Zachariasen, "The atomic arrangement in glass," *J. Am. Chem. Soc.* **54** [10] 3841-3851 (1932).
 14. L. Bressel, D. de Ligny, C. Sonnevile, V. Martinez-Andrieux, and S. Juodkazis, "Laser-induced structural changes in pure GeO_2 glasses," *J. Non-Cryst. Solids* **357** [14] 2637-2640 (2011).
 15. L. Bressel, D. de Ligny, C. Sonnevile, V. Martinez, V. Mizeikis, R. Buividas, and S. Juodkazis, "Femtosecond laser induced density changes in GeO_2 and SiO_2 glasses: fictive temperature effect," *Opt. Mater. Exp.* **1** [4] 605-613 (2011).
 16. L. Bressel, D. de Ligny, E. G. Gamaly, A. V. Rode, and S. Juodkazis, "Observation of O_2 inside voids formed in GeO_2 glass by tightly-focused fs-laser pulses," *Opt. Mater. Exp.* **1** [6] 1150-1158 (2011).

17. M. Shimizu, M. Sakakura, S. Kanehira, M. Nishi, Y. Shimotsuma, K. Hirao, and K. Miura, “Formation mechanism of element distribution in glass under femtosecond laser irradiation,” *Opt. Lett.* **36** [11] 2161-2163 (2011).
18. M. Sakakura, T. Kurita, M. Shimizu, K. Yoshimura, Y. Shimotsuma, N. Fukuda, K. Hirao, and K. Miura, “Shape control of elemental distributions inside a glass by simultaneous femtosecond laser irradiation at multiple spots,” *Opt. Lett.* **38** [23] 4939-4942 (2013).
19. E. Bricchi, B. G. Klappauf, and P. G. Kazansky, “Form birefringence and negative index change created by femtosecond direct writing in transparent materials,” *Opt. Lett.* **29** [1] 119-121 (2004).
20. Y. Shimotsuma, M. Sakakura, P. G. Kazansky, M. Beresna, J. Qiu, K. Miura, and K. Hirao, “Ultrafast manipulation of self-assembled form birefringence in glass,” *Adv. Mater.* **22** [36] 4039-4043 (2010).
21. M. Birnbaum, “Semiconductor surface damage produced by ruby lasers,” *J. Appl. Phys.* **36** [11] 3688-3689 (1965).
22. J. Bonse, J. Krüger, S. Höhm, and A. Rosenfeld, “Femtosecond laser-induced periodic surface structures,” *J. Laser Appl.* **24** [4] 042006 7pp. (2012).
23. J. E. Sipe, J. F. Young, J. S. Preston, and H. M. van Driel, “Laser-induced periodic surface structure. I. Theory,” *Phys. Rev. B* **27** [2] 1141-1154 (1983).
24. M. Hashida, Y. Ikuta, Y. Miyasaka, S. Tokita, and S. Sakabe, “Simple formula for the interspaces of periodic grating structures self-organized on metal surfaces by femtosecond laser ablation,” *Appl. Phys. Lett.* **102** [17] 174106 4pp. (2013).
25. Y. Shimotsuma, K. Hirao, J. Qiu, and P. G. Kazansky, “Nano-modification inside transparent

- materials by femtosecond laser single beam,” *Mod. Phys. Lett. B* **19** [5] 225-238 (2005).
26. S. Richter, C. Miese, S. Döring, F. Zimmermann, M. J. Withford, A. Tünnermann, and S. Nolte, “Laser induced nanogratings beyond fused silica - periodic nanostructures in borosilicate glasses and ULE,” *Opt. Mater. Express* **3** [8] 1161-1166 (2013).
27. V. Bhardwaj, E. Simova, P. Rajeev, C. Hnatovsky, R. Taylor, D. Rayner, and P. Corkum, “Optically produced arrays of planar nanostructures inside fused silica,” *Phys. Rev. Lett.* **96** [5] 057404 4pp. (2006).
28. Y. Shimotsuma, T. Asai, M. Sakakura, and K. Miura, “Femtosecond-laser nanostructuring in glass,” *J. Laser Micro/Nanoeng.* **9** [1] 31-36 (2014).
29. F. Zhang, H. Zhang, G. Dong, and J. Qiu, “Embedded nanogratings in germanium dioxide glass induced by femtosecond laser direct writing,” *J. Opt. Soc. Am. B* **31** [4] 860-864 (2014).
30. Q. Sun, H. Jiang, Y. Liu, Y. Zhou, H. Yang, and Q. Gong, “Effect of spherical aberration on the propagation of a tightly focused femtosecond laser pulse inside fused silica,” *J. Opt.* **7** [11] 655-659 (2005).
31. Y. Shimotsuma, K. Hirao, J. Qiu, K. Miura, “Nanofabrication in transparent materials with a femtosecond pulse laser,” *J. Non-Cryst. Solids* **352** [6-7] 646-656 (2006).
32. E. N. Glezer and E. Mazur, “Ultrafast-laser driven micro-explosions in transparent materials,” *Appl. Phys. Lett.* **71** [7] 882-884 (1997).
33. M. Sakakura, M. Shimizu, Y. Shimotsuma, K. Miura, and K. Hirao, “Temperature distribution and modification mechanism inside glass with heat accumulation during 250 kHz irradiation of femtosecond laser pulses,” *Appl. Phys. Lett.* **93** [23] 231112 3pp. (2008).
34. M. Shimizu, M. Sakakura, M. Ohnishi, Y. Shimotsuma, T. Nakaya, K. Miura, and K. Hirao,

- “Mechanism of heat-modification inside a glass after irradiation with high-repetition rate femtosecond laser pulses,” *J. Appl. Phys.* **108** [7] 073533 10pp. (2010).
35. S. M. Eaton, H. Zhang, P. R. Herman, F. Yoshino, L. Shah, J. Bovatsek, and A. Y. Arai, “Heat accumulation effects in femtosecond laser-written waveguides with variable repetition rate,” *Opt. Express* **13** [12] 4708-4716 (2005).
36. C. Corbari, A. Champion, M. Gecevičius, M. Beresna, Y. Bellouard, and P. G. Kazansky, “Femtosecond versus picosecond laser machining of nano-gratings and micro-channels in silica glass,” *Opt. Express* **21** [4] 3946-3958 (2013).
37. C. Hnatovsky, R. S. Taylor, P. P. Rajeev, E. Simova, V. R. Bhardwaj, D. M. Rayner, and P. B. Corkum, “Pulse duration dependence of femtosecond-laser-fabricated nanogratings in fused silica,” *Appl. Phys. Lett.* **87** [1] 014104 3pp. (2005).
38. C. Mauclair, M. Zamfirescu, J. P. Colombier, G. Cheng, K. Mishchik, E. Audouard, and R. Stoian, “Control of ultrafast laser-induced bulk nanogratings in fused silica via pulse time envelopes,” *Opt. Express* **20** [12] 12997-13005 (2012).
39. J. Canning, M. Lancry, K. Cook, A. Weickman, F. Brisset, and B. Poumellec, “Anatomy of a femtosecond laser processed silica waveguide,” *Opt. Mater. Exp.* **1** [5] 998-1008 (2011).
40. S. Richter, A. Plech, M. Steinert, M. Heinrich, S. Döring, F. Zimmermann, U. Peschel, E. Bernhard Kley, A. Tünnermann, and S. Nolte, “On the fundamental structure of femtosecond laser-induced nanogratings,” *Laser Photon. Rev.* **6** [6] 787-792 (2012).
41. S. P. Sharma, V. Oliveira, P. Herrero, and R. Vilar, “Internal structure of the nanogratings generated inside bulk fused silica by ultrafast laser direct writing,” *J. Appl. Phys.* **116** [5] 053106 6pp. (2014)

42. M. Born and E. Wolf, *Principles of Optics*. Cambridge University Press, Cambridge, U.K., 1999.
43. M. M. Braun and L. Pilon, “Effective optical properties of non-absorbing nanoporous thin films,” *Thin Solid Films* **496** [2] 505-514 (2006).
44. M. Rothschild, D. J. Ehrlich, and D. C. Shaver, “Effects of excimer laser irradiation on the transmission, index of refraction, and density of ultraviolet grade fused silica,” *Appl. Phys. Lett.* **55** [13] 1276-1278 (1989).
45. M. K. Schurman and M. Tomozawa, “Equilibrium oxygen vacancy concentrations and oxidant diffusion in germania, silica, and germania-silica glasses,” *J. Non-Cryst. Solids* **202** [1-2] 93-106 (1996).
46. J. Zhang, M. Gecevičius, M. Beresna, and P. G. Kazansky, “Seemingly unlimited lifetime data storage in nanostructured glass,” *Phys. Rev. Lett.* **112** [3] 033901 5pp. (2014).

Figure captions

Figure 1. Optical micrographs of the modified regions inside GeO₂ glass induced by the femtosecond laser pulses with various pulse energies. The rows of (a) and (b) show top and side views. k_w indicates the direction of laser propagation. Scale bars are 5 μm . The laser parameters were as follow: 800 nm, 50 fs, 250 kHz, 250000 pulses, 0.80 NA.

Figure 2. Sequential Raman spectra of the structural changes as a function of the pulse energy. The Raman spectrum of the initial glass (Before) is also shown. Inset graph shows the variation of Raman peak intensities at 420, 520, and 1555 cm^{-1} with respect to the initial intensities ($I^{\text{after}}/I^{\text{before}}$) as a function of the pulse energy.

Figure 3. The phase retardation of birefringence induced by the femtosecond laser pulses with various pulse repetition rate (a) and pulse width (b). The laser parameters were as follow: (a) 1030 nm, 176 fs, 0.24 μJ , 250000 pulses, 0.80 NA; (b) 1030 nm, 200 kHz, 0.15 μJ , 250000 pulses, 0.80 NA.

Figure 4. SEIs (a, c) and BEIs (b, d) of GeO₂ glass surface processed close to the laser focal position by FIB. The magnification of the upper (a, b) and lower (c, d) images is 7500 \times and 50000 \times , respectively. The laser parameters were as follow: 800 nm, 50 fs, 0.2 μJ , 250 kHz, 250000 pulses, 0.80 NA.

Figure 5. SEIs on the cleaved surface of the laser traces written by the femtosecond laser pulses with pulse energy of 0.2 μJ (a-d) or 2.4 μJ (e-h) for each writing laser polarization. The polarization direction (E) was perpendicular (a, b, e, f) or parallel (c, d, g, h) to the writing direction (S). The high magnification SEIs in the dotted area in (a, c, e, g) are also shown in (b, d, f, h), respectively. Scale bars in the low and high magnification images are 5 μm and 1 μm , respectively. The laser parameters were as follow: 800 nm, 50 fs, 250 kHz, 250 $\mu\text{m/s}$, 0.80 NA. Symbol of k_w indicates the laser propagation direction.

Figure 6. SEIs of the cleaved sample surfaces of the modified regions in GeO_2 glass (a, b) and SiO_2 glass (c, d) created by the femtosecond laser pulses with a pulse energy of 0.2 μJ (a, c) or 0.4 μJ (b, d). The insets in each figure show the high magnification SEIs in the area surrounded by dotted square. The scale bars are 200 nm.

Figure 7. Schematic of the nanogratings formed in the irradiated volume. n_{bg} : refractive index of the initial glass, n_1, n_2 : local refractive indices of nanoplatelet, $f = t_1/\Lambda$: filling factor, Λ : period of the nanograting, t_1 : width of the region with index n_1 , $n_{\text{void}} = 1$: refractive index of the nanopore, n_{defect} : refractive index of the region surrounding the nanopores.

Figure 8. Phase retardation (a) and birefringence (b) of the induced structures in GeO_2 and SiO_2 glass as a function of the laser pulse energy.

Figure 9. Optical (upper rows) and polarization (lower rows) microscope images of the modified

regions inside GeO_2 glass by the femtosecond laser pulse with the pulse energy of $0.2 \mu\text{J}$ (row (a)) or $2.4 \mu\text{J}$ (row (b)) after successive annealing at various temperature. Scale bars are $10 \mu\text{m}$. (c) Arrhenius plots of the induced phase retardation inside GeO_2 and SiO_2 glass by the femtosecond laser pulses with a pulse energy of $0.2 \mu\text{J}$ and $0.4 \mu\text{J}$, respectively, as a function of the annealing temperature for 1 hour.

Table

Table 1. Parameters for calculation of local refractive index change in SiO₂ and GeO₂ glass

Material	SiO ₂ glass	GeO ₂ glass	Material	SiO ₂ glass	GeO ₂ glass
n_{bg}	1.454	1.645	n_{pore}	1	1
t_1^*	30 nm	50 nm	n_{defect}	1.454	1.645
Λ^{**}	200 nm	250 nm	ϕ	0.20	0.15
$f = t_1/\Lambda$	0.15	0.20	$n_1 - n_{bg}$	-0.092	-0.098
Δn	0.003	0.005	$n_2 - n_{bg}$	+0.035	+0.048

* t_1 : the width of the region with index of n_1 ; ** Λ : the period of nanogratings



0.08 μJ

0.3 μJ

0.4 μJ

0.8 μJ

2.4 μJ

京都大学

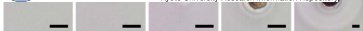
京都大学学術情報リポジトリ

紅

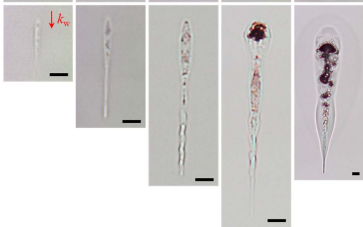
KYOTO UNIVERSITY

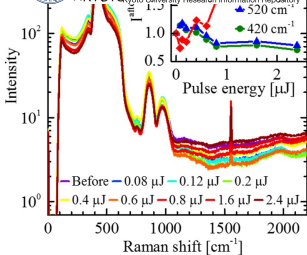
Kyoto University Research Information Repository

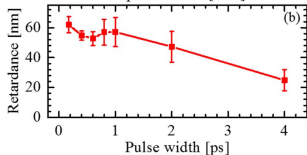
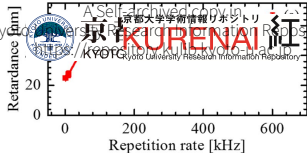
(a)



(b)







2 μm

2 μm

(c)

200 nm

(d)

200 nm

